



4.2 Low-Order & Focal Plane Wavefront Sensing and Control

Kelsey Miller

1 Low-Order Wavefront Sensing (LOWFS)

1.1 LOWFS theory: Low-order wavefront sensing (LOWFS) is a coronagraphic wavefront sensing technique designed to sense pointing errors and other low-order wavefront aberrations using starlight that would normally just be rejected by the coronagraph. In a Lyot coronagraph, a mask is placed at the focal plane which diffracts starlight outside the geometrical pupil into a downstream pupil plane at which a Lyot mask, an undersized replica of the entrance pupil, is placed. In traditional coronagraphs, starlight is simply blocked by both of these masks, but for LOWFS, that rejected starlight from either the focal plane and the reimaged pupil plane is reflected, respectively, by a reflective focal plane mask (FPM) as well as a reflective Lyot stop, each toward a reimaged focal plane. The resulting PSFs from the starlight rejected by both masks are imaged by separate detectors and used to measure the low-order aberrations. LOWFS is a linear wavefront reconstructor that fits post-AO wavefront residuals to a command matrix built by registering the response of these rejected starlight PSFs to aberrations injected into the system by a deformable mirror (DM). This technique relies on the assumption that if the post-AO wavefront residuals are $\ll 1$ radian rms then the intensity variations in the reflected light are a linear combination of the low-order aberrations occurring upstream of the focal plane mask. LOWFS has been successfully deployed on-sky by the Subaru Coronagraphic Extreme AO (SCExAO) team, who are contributors to the MagAO-X effort. (1)

1.2 LOWFS for MagAO-X: In the MagAO-X system, a separate LOWFS arm has been designed to sense and correct pointing, tip/tilt, and other low-order modes. Slightly different from the original technique described above, the MagAO-X LOWFS system will use the stellar light leakage term from the vAPP coronagraph (see Section 5.5 Vector apodizing phase plate coronagraph for MagAO-X) as the LOWFS signal. To build the LOWFS control loop around this signal, an ALPAO deformable mirror (DM) with 97 actuators has been selected to be the wavefront corrector to compensate these low-order errors. The MagAO-X instrument will take full advantage of the ability to do wavefront correction with all 97 accessible modes. To do this, LOWFS must be sensitive to all 97 modes; this is accomplished in part by defocusing the LOWFS PSF which broadens the area on the detector over which the modes can be sensed. Due to their smaller uncompensated residual wavefront fitting error (as compared to Zernike modes), atmospheric Karhunen-Loeve (KL) modes were chosen to build a 97 mode reconstruction matrix. The following document demonstrates the MagAO-X LOWFS ability to sense and control 97 KL modes individually and in random combinations, and its ability to use a KL modal basis set to sense and correct random Kolmogorov phase errors. The reflective Lyot stop PSF was defocused by $0.1 \mu\text{m}$ for these demonstrations.

1.3 LOWFS elements:

1.3.1 Stellar signal: As previously mentioned, the MagAO-X system will rely on the signal from the stellar light leakage term from the vAPP coronagraph (Fig 1). In terms of spatial frequency sensitivity, the LOWFS control loop built around the response of the light leakage PSF will be similar to both the reflected FPM and reflected Lyot



mask cases described previously. This is because the signal from the light leakage term in the vAPP case is not diffracted or blocked by any masks; instead, the stellar leakage PSF is passed directly to a detector, thereby containing both the low and the high spatial frequency content that would be seen by the reflective FPM and Lyot mask cases. The reflective Lyot mask case was chosen to for the following demonstrations of LOWFS on MagAO-X as it was under development for use with the PIAACMC, and the underlying principle is the same. The reflective Lyot mask used for these simulations is shown in Fig 2. The signal from this reflected starlight contains the low, mid, and high spatial frequency content (see Section 1.4 for verification) that will be seen with the vAPP stellar leakage PSF.

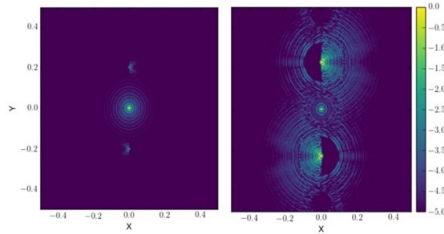


Figure 1: LOWFS signal from the vAPP stellar light leakage term (center PSF) shown between the two coronagraphic PSFs. See Section 5.5 Vector apodizing phase plate coronagraph for MagAO-X for details.

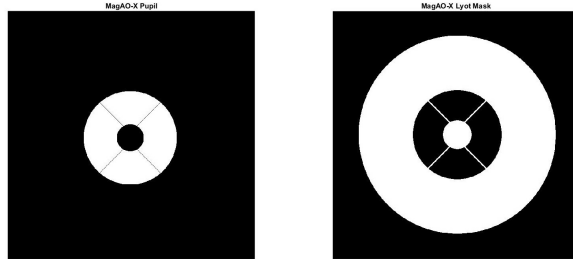


Figure 2: MagAO-X masks: Entrance pupil mask (left) and the reflective Lyot stop used for the following LOWFS simulations (right)

1.3.2 Deformable mirror: In the MagAO-X LOWFS arm, the low-order aberrations sensed using the starlight reflected by the Lyot mask will be corrected using an ALPAO DM 97-15 (see full spec sheet for this DM below in Figure 3.). The ALPAO DM is circular and 13.5 mm in diameter and has 97 actuators across the full pupil. This will allow for LOWFS correction with up to 97 individual modes. This DM has been modeled using the mirror's gaussian influence functions for use in the following simulation work demonstrating the MagAO-X LOWFS ability to sense and correct 97 modes.



MagAO-X Preliminary Design

4.2: LO/FP WFS&C

Doc #: MagAOX-PDR-001
Date: 2017-04-22
Status: Rev. 0.0
Page: 3 of 16



| | DM 69 | DM 88 | DM 97-08 | DM 97-15 | DM 241 | DM 277 | DM 468 | DM 820 |
|--------------------------------|------------------------------|-------|----------|----------|--------|--------|--------|--------|
| Number of actuators | 69 | 88 | 97 | 97 | 241 | 277 | 468 | 820 |
| Pupil diameter (mm) | 10.5 | 20.0 | 7.2 | 13.5 | 37.5 | 24.5 | 33.0 | 45.0 |
| Pitch (mm) | 1.5 | 2.5 | 0.8 | 1.5 | 2.5 | | 1.5 | |
| Mirror best flat in close loop | 7.0nm RMS (no print through) | | | | | | | |
| Wavefront tip/tilt stroke (PV) | 60μm | 40μm | 80μm | 60μm | 40μm | | 15μm | |
| Settling time (at +/-10%) | 800μs | | 1.6ms | 800μs | 1.6ms | | 500μs | |

Figure 3: ALPAO DM 97-15 with specifications (2)

1.4 Sensitivity and correction with 97 Karhunen-Loeve modes: To demonstrate the MagAO-X LOWFS ability to sense and correct 97 modes, a Karhunen-Loeve (KL) modal basis set was derived using Fourier modes. (All 97 KL modes can be seen in Figure 4.)

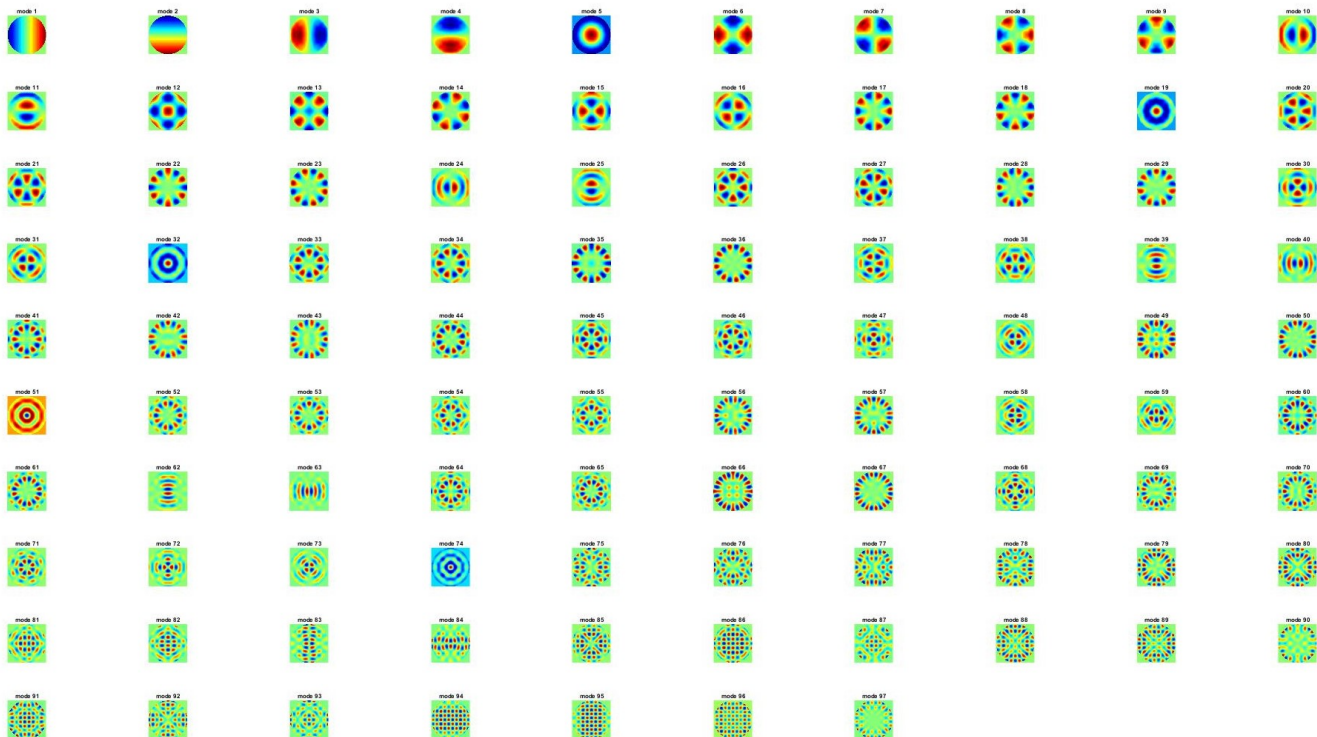


Figure 4: 97 KL modes sensed in the following section

The LOWFS response matrix used in the LOWFS control loop was then constructed using these 97 KL modes. To build the LOWFS response matrix, each of these individual modes was then applied to the model ALPAO DM, and the PSF formed by the light reflected by the Lyot mask was recorded for each mode. (All 97 PSFs can be seen in Figure 5)



MagAO-X Preliminary Design 4.2: LO/FP WFS&C

Doc #: MagAOX-PDR-001
 Date: 2017-04-22
 Status: Rev. 0.0
 Page: 4 of 16

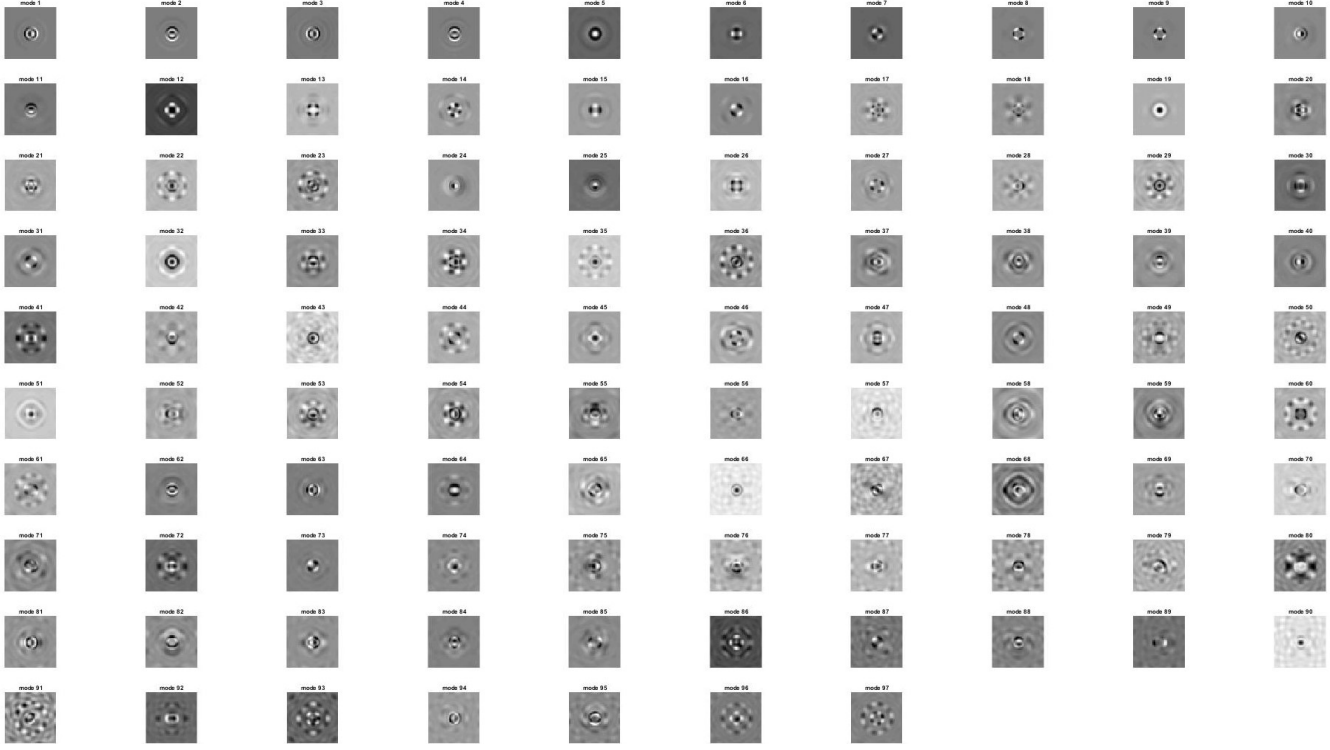


Figure 5: The LOWFS PSF for all 97 KL modes

Each of these PSFs is then reshaped into a single column vector in the LOWFS response matrix. The command matrix used in the LOWFS control loop is then the pseudo-inverse of this response matrix. This command matrix was then used in the following simulations to show the MagAO-X LOWFS ability to sense and control these modes.

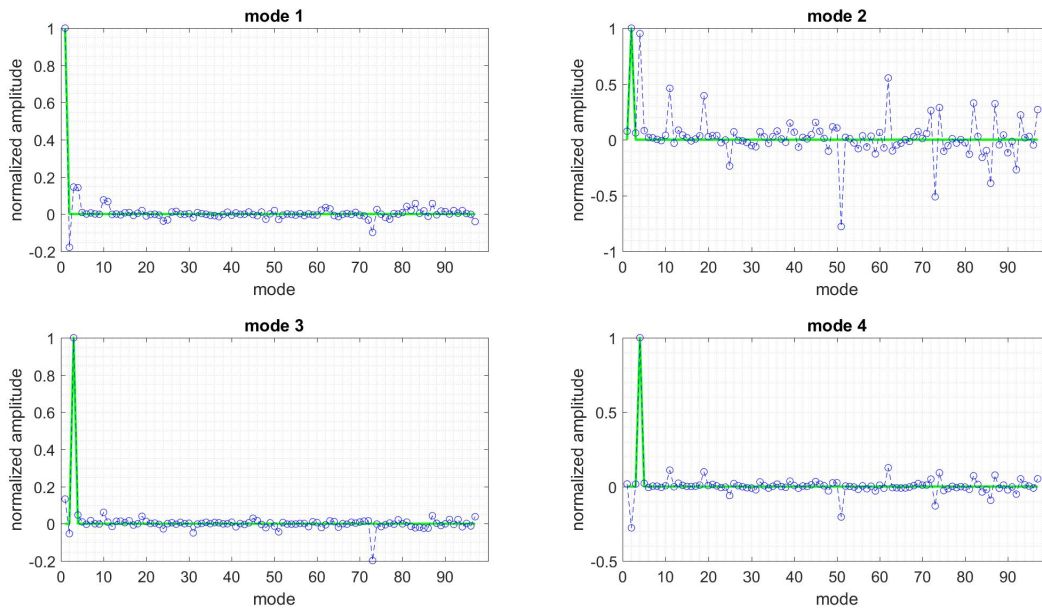
1.4.1 Sensing and correcting individual KL modes: In the following section, each of the 97 KL modes shown in Figure 4 was applied individually to the ALPAO DM model and sensed using the model MagAO-X LOWFS system. Each plot shows the normalized amplitude of the single KL mode that was applied (in green) and the normalized amplitude of each KL mode in the LOWFS response (in blue). For this simulation, the LOWFS PSF was defocused by $0.1 \mu\text{m}$. It should be noted that the LOWFS response to certain modes is noisier than others. This is due to the fact that, for mid-spatial frequencies, there is a tradeoff between coronagraph inner working angle (IWA), transmission at small angles and LOWFS sensitivity. With a low-IWA coronagraph with good throughput outside of the IWA, LOWFS can only measure a few modes with good sensitivity.



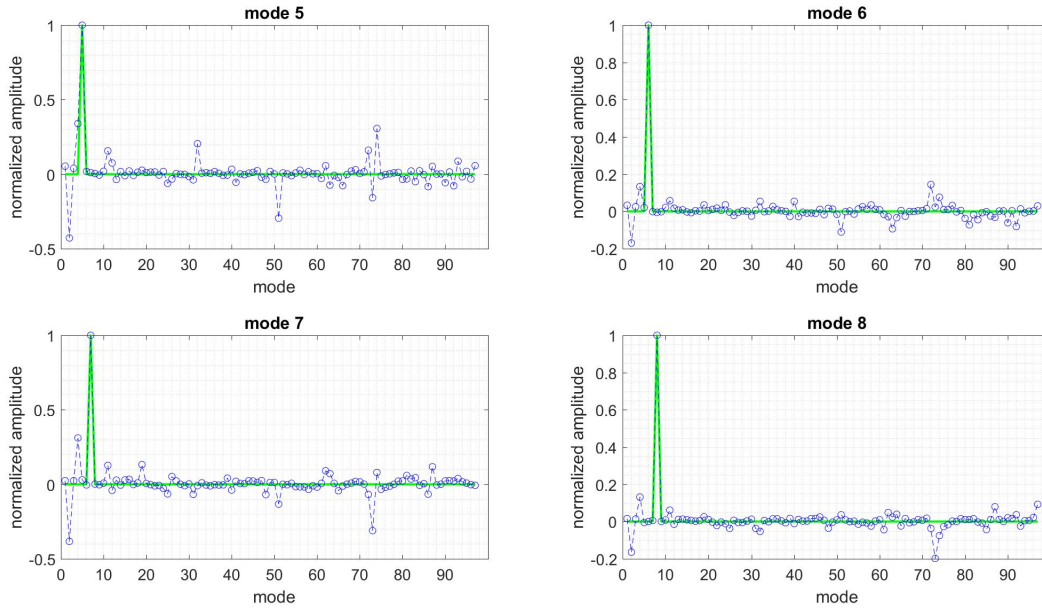
MagAO-X Preliminary Design

4.2: LO/FP WFS&C

Doc #: MagAOX-PDR-001
Date: 2017-04-22
Status: Rev. 0.0
Page: 5 of 16



(a) Sensitivity to KL modes 1 - 4



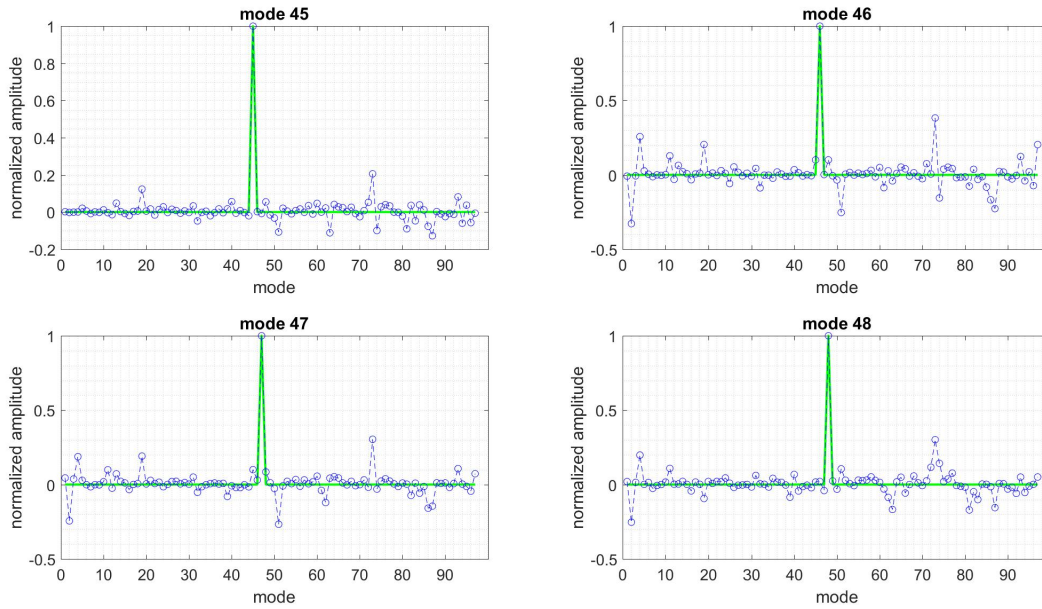
(b) Sensitivity to KL modes 5 - 8

Figure 6: LOWFS response to low-order KL modes with low spatial frequency content

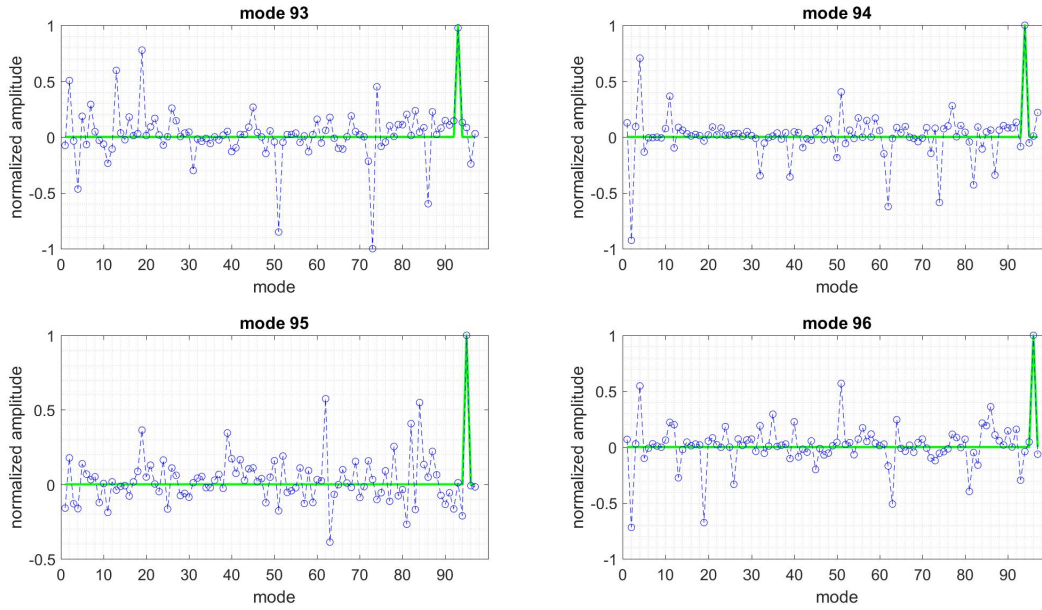


MagAO-X Preliminary Design
4.2: LO/FP WFS&C

Doc #: MagAOX-PDR-001
Date: 2017-04-22
Status: Rev. 0.0
Page: 6 of 16



(a) Sensitivity to KL modes 45 - 48



(b) Sensitivity to KL modes 93 - 96

Figure 7: LOWFS response to mid- and high-order KL modes with mid and high spatial frequency content



1.4.2 Sensing and correcting a combination of KL modes: LOWFS is capable of correcting low-order aberrations within spatial frequency bands to which the technique is sensitive. One demonstration of this ability is shown below. The MagAO-X PSF was aberrated by a random combination of 10 of the 97 KL modes injected into the pupil and then corrected by LOWFS using the full 97 KL mode command matrix. In Figure 8, this 10 KL mode aberration is shown to the left. The LOWFS response to cancel this aberration is applied to the model ALPAO DM in the center image, and the residual wavefront error after the LOWFS correction is shown to the right.

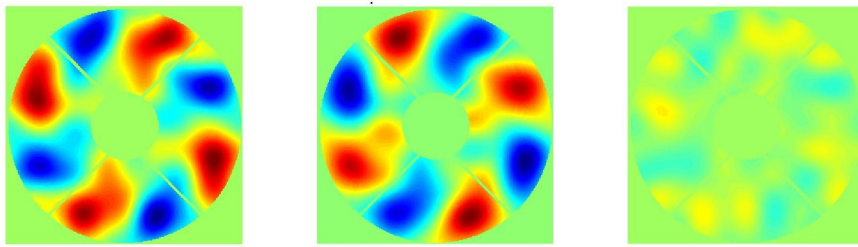


Figure 8: Injected 10 KL mode aberration (left). Applied LOWFS correction (center). Residual phase error after LOWFS (right).

The results from this test are visualized in Figure 9 by showing the LOWFS PSFs and the PSFs seen at the science detector. In the top row, the $0.1 \mu\text{m}$ defocused LOWFS PSF used for sensing the aberration in the pupil is shown. The PSF to the left is aberrated by the random 10 KL mode phase aberration injected into the pupil shown in the left panel of Figure 8. The PSF to the right is the final LOWFS-corrected PSF after the DM has compensated the injected aberration by applying the shape seen in the center panel of Figure 8. In the bottom row, the aberrated PSF at the science detector is shown to the left, and the LOWFS-corrected science PSF is shown to the right. The center PSF in the top and bottom rows of Figure 9 are the differences between the corrected and aberrated LOWFS and science PSFs respectively.



MagAO-X Preliminary Design

4.2: LO/FP WFS&C

Doc #: MagAOX-PDR-001
Date: 2017-04-22
Status: Rev. 0.0
Page: 8 of 16

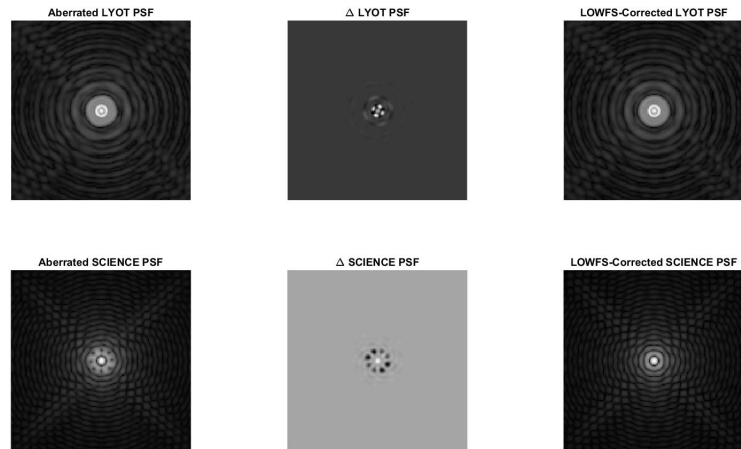


Figure 9: Correction of 10 applied random KL modes using full 97 mode response matrix. Shows the aberrated and corrected LOWFS PSF (top row), and the the aberrated and corrected science PSF (bottom row)

Figure 8 shows the normalized amplitudes of the 10 KL modes in the injected aberration (in green) and the normalized amplitudes of all 97 KL modes in the LOWFS response to this aberration.

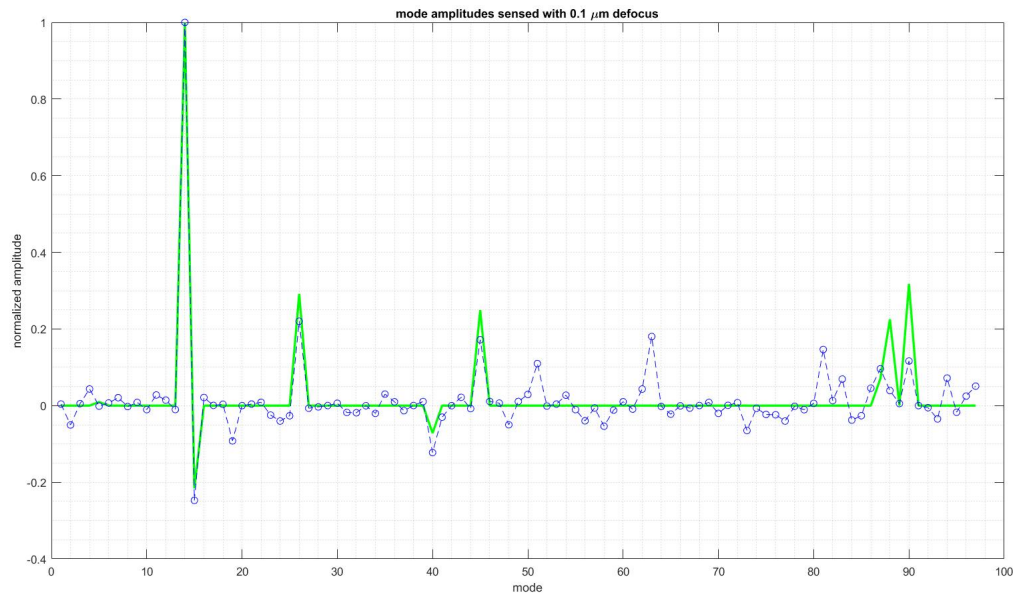


Figure 10: The amplitudes of the 10 applied random KL modes (green) and the amplitude of each mode in the LOWFS response (blue).



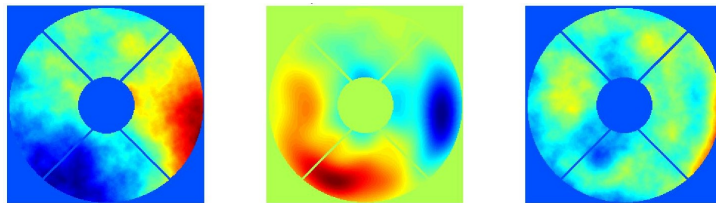
1.4.3 Sensing and correcting random Kolmogorov phase: In Section 5.1 Optics Specifications, subsection 5.3 Spec comparison, the PSDs for all of the optics in the LOWFS arm of MagAO-X were summed to determine the total power that will be added by the optical surfaces of these noncommon path (NCP) optics. This added power must be actively sensed and corrected by the LOWFS system. To ensure that the correction of this added power due to static and noncommon path (NCP) does not saturate the ALPAO DM, the stroke required to impose these corrections was analyzed (see Section 5.1 Optics Specifications, subsection 5.4 DM stroke). For the highest precision optics with a surface quality of $\lambda/200$, the RMS surface error that must be sensed and corrected by the LOWFS system is 9.6 nm. To prove that the MagAO-X LOWFS system is capable of removing this power, a modified Kolmogorov phase screen with a $\frac{\beta}{k^\alpha}$ PSD was simulated in the system pupil plane to model the combined NCP optics PSD. (In this PSD, k is the spatial frequency, β is a normalization constant, and α is the PSD index.) To model the optical surface PSD, α was chosen to be 2, and the surface precision of the phase screen was set to be 9.6 nm RMS. Using this model, it was then shown that, in the presence of photon noise, the MagAO-X LOWFS system will be capable of sensing and correcting this 9.6 nm RMS optical surface error for multiple stellar magnitudes.

The LOWFS response and correction of the 9.6 nm RMS optical surface error was run for stellar magnitudes 0, 5, 8, 10, and 12 and the frequency at which the LOWFS loop must run to obtain this correction for each stellar magnitude. The LOWFS response matrix was built using the first 20 KL modes. Results from these tests are shown below.

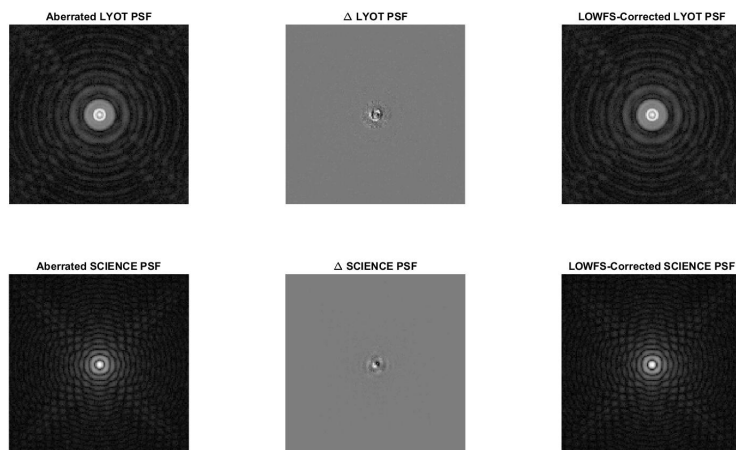


MagAO-X Preliminary Design
4.2: LO/FP WFS&C

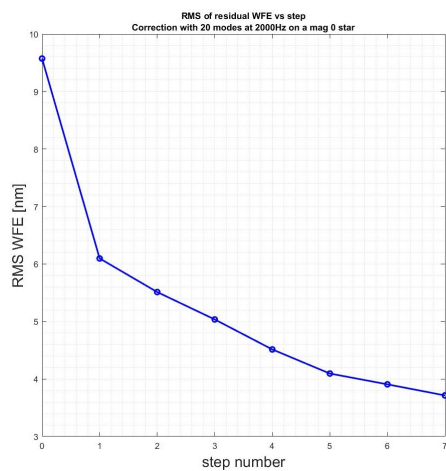
Doc #: MagAOX-PDR-001
Date: 2017-04-22
Status: Rev. 0.0
Page: 10 of 16



(a) (Left) 9.6 nm RMS optical surface (Center) LOWFS correction applied on ALPAO DM (Right) Residual error after LOWFS correction



(b) (Top row) LOWFS PSF before and after correction. (Bottom row) Science PSF before and after correction.



(c) Residual RMS error after LOWFS correction step in nm.

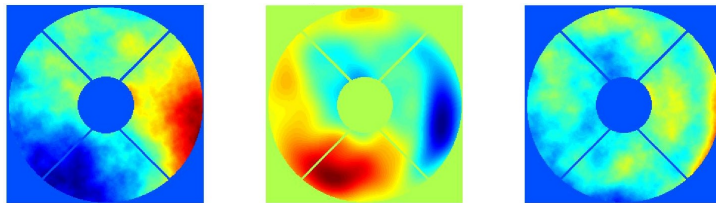
Figure 11: LOWFS correction running at 2 kHz on a 0 magnitude star. Residual error is less than 3.8 nm RMS.



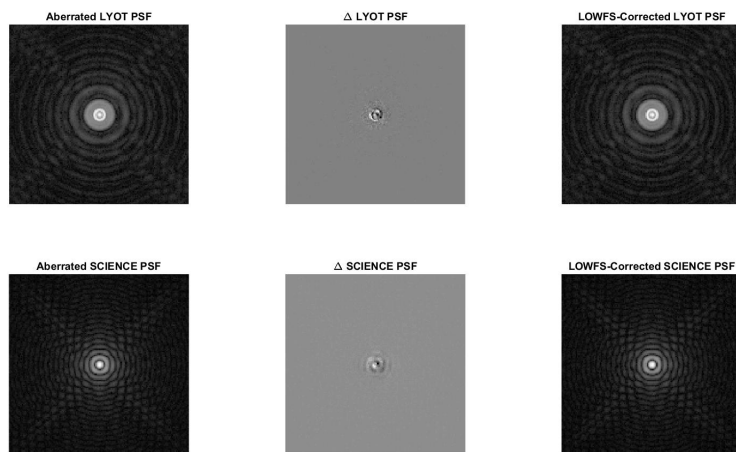
MagAO-X Preliminary Design

4.2: LO/FP WFS&C

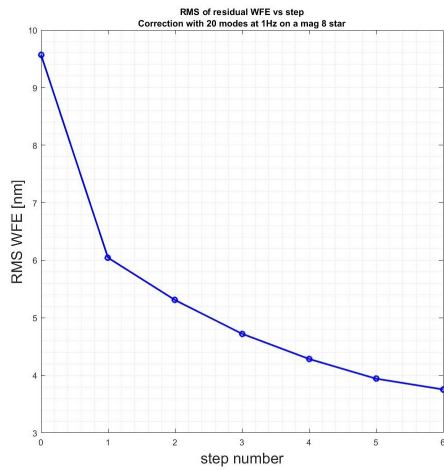
Doc #: MagAOX-PDR-001
Date: 2017-04-22
Status: Rev. 0.0
Page: 11 of 16



(a) (Left) 9.6 nm RMS optical surface (Center) LOWFS correction applied on ALPAO DM (Right) Residual error after LOWFS correction



(b) (Top row) LOWFS PSF before and after correction. (Bottom row) Science PSF before and after correction.



(c) Residual RMS error after LOWFS correction step in nm.

Figure 12: LOWFS correction running at 1 Hz on an 8 magnitude star. Residual error is less than 3.8 nm RMS.



Figure 13 shows the maximum frequency at which the LOWFS loop can be run for stellar magnitudes 0, 5, 8, 10, and 12 while correcting the 9.6 nm RMS surface error.

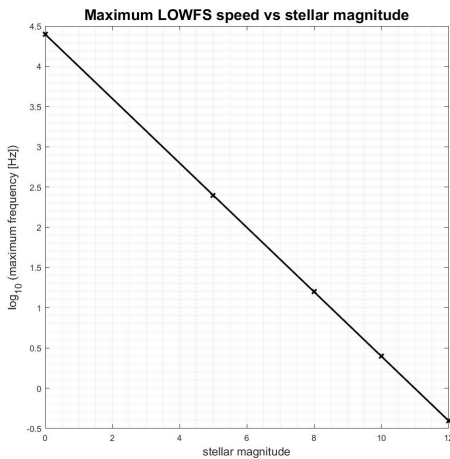


Figure 13: Stellar magnitude vs the \log_{10} scale maximum LOWFS frequency for sensing and correcting 9.6 nm RMS surface error

This plot shows that, for a magnitude 0 star, the maximum frequency at which LOWFS can be run is 25 kHz. For a magnitude 12 start this decreases to 0.4 Hz. For all five stellar magnitudes, LOWFS is capable of sensing and correcting the required 9.6 nm RMS error induced by the NCP optics surface PSD.

1.5 Sensing and correcting quadrant piston error: A common problem that has been seen on-sky by multiple observatories is phase-wrapping error that appears as a piston term in wavefront sensor correction. This piston term appears across entire sectors within the entrance pupil that are defined by the projection of the support structures known as 'spiders' in the pupil plane. This piston error is not sensed by the wavefront sensor and causes the correction to walk-off. MagAO-X intends to sense and correct this error using LOWFS. In the section below, a 50 nm piston error was induced in each of the four MagAO pupil quadrants. LOWFS was then used to sense this piston and suppress it. The injected piston and LOWFS response in each quadrant can be seen in Figure 14.



MagAO-X Preliminary Design
4.2: LO/FP WFS&C

Doc #: MagAOX-PDR-001
 Date: 2017-04-22
 Status: Rev. 0.0
 Page: 13 of 16

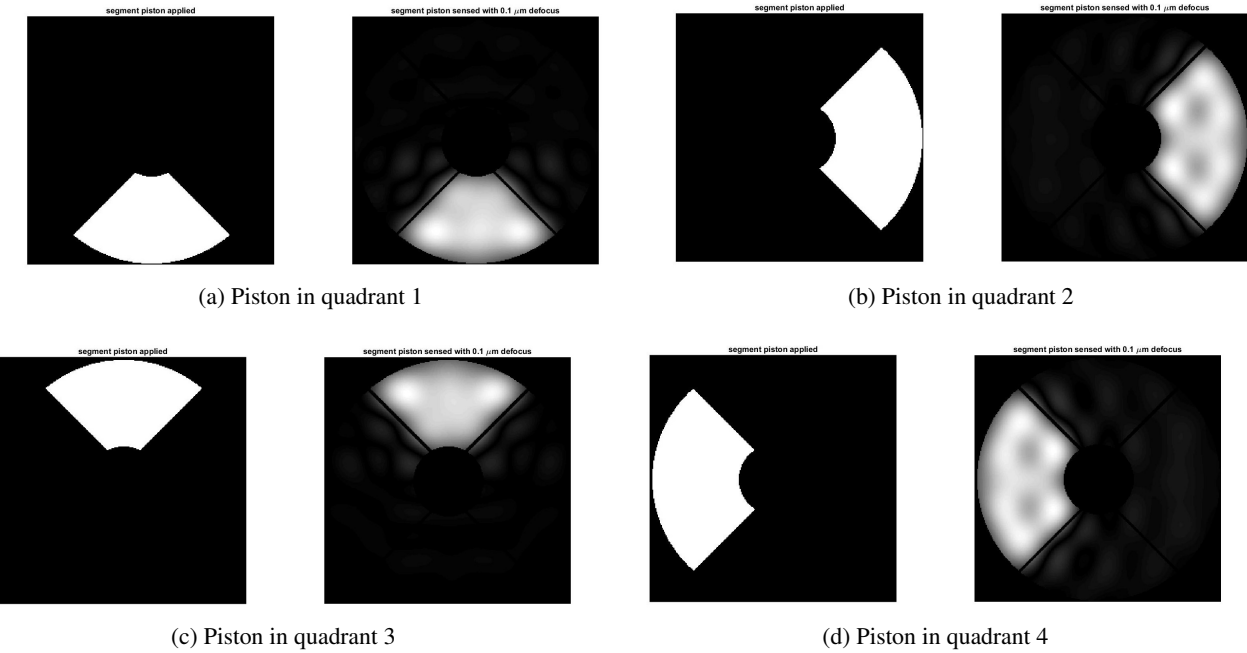


Figure 14: The applied piston error in each quadrant (left images) and the resulting piston error sensed by LOWFS (right images)

The normalized amplitude of the applied piston (in green) and the normalized amplitude of the LOWFS response to the injected piston (in blue) are shown in Figure 15.

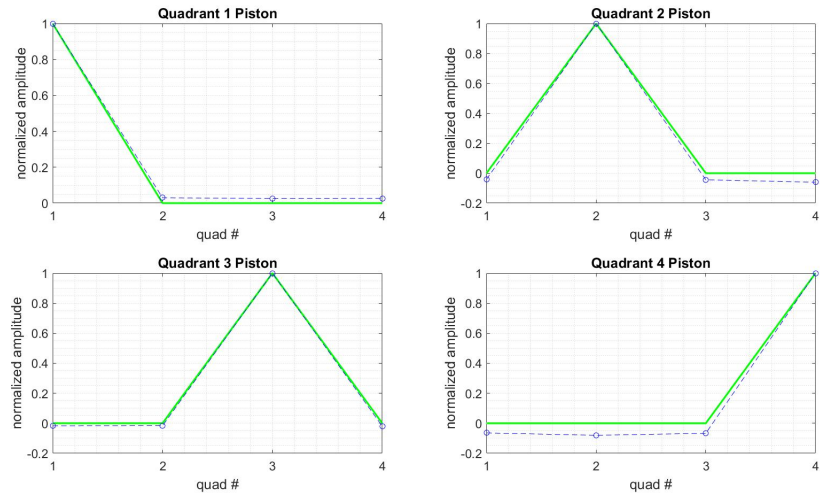


Figure 15: The applied piston error in each quadrant (green) and the piston error sensed by LOWFS (blue) for each of the four quadrants



For quadrant 4, the effect of the piston error on the LOWFS PSF (top row) and science PSF (bottom row) can be seen in Figure 16. The images to the left show the aberration induced in the LOWFS and science PSFs by the piston error, and the right images show the resulting LOWFS corrections.

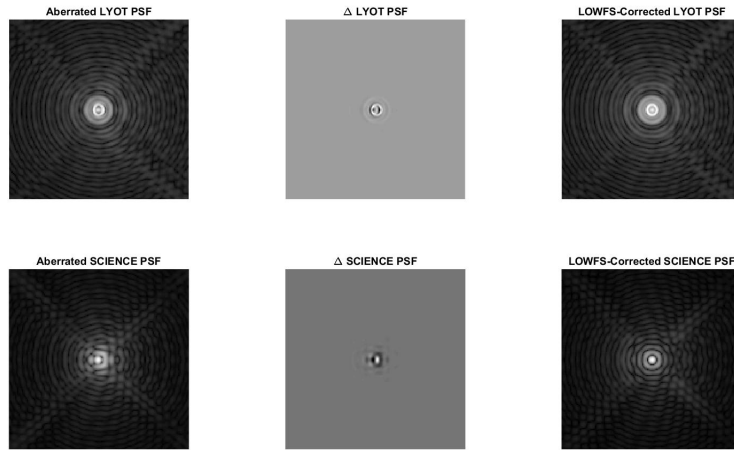


Figure 16: Correction of piston in quadrant 4. Shows the aberrated and corrected LOWFS PSF (top row), and the the aberrated and corrected science PSF (bottom row)

These results are a promising indicator that MagAO-X will be capable of sensing and canceling this known piston error using LOWFS.

2 Focal Plane Wavefront Sensing (FPWFS)

2.1 FPWFS theory: To directly image exoplanets, high-precision wavefront control is required. This required precision cannot be obtained by wavefront sensor systems like LOWFS that branch off from the main science beam since, in doing so, they introduce optics to the seen by the wavefront sensor that are not seen by the science detector. The resulting differences between the wavefront sensor (WFS) and science detector caused by these optics in the separate wavefront sensor arm are known as non-common path (NCP) errors. NCP errors limit the ability of the wavefront sensor to achieve the wavefront control precision required for techniques such as electric field conjugation (EFC) that are essential for exoplanet direct imaging.(3)

Focal plane wavefront sensing (FPWFS) is capable of achieving the necessary high precision by using the science detector as the WFS, thereby avoiding NCP errors. The FPWFS control loop consists of the science camera/WFS and the deformable mirror (DM) which modulates the field at the science camera.

2.2 FPWFS for direct exoplanet imaging: The MagAO-X instrument will feature a Boston Micromachine 2K DM as its main wavefront corrector. This DM will allow for FPWFS with access to high spatial frequencies. With this DM, MagAO-X will be capable of creating regions of deep contrast (a dark hole) within which an orbiting



exoplanet can be directly imaged.

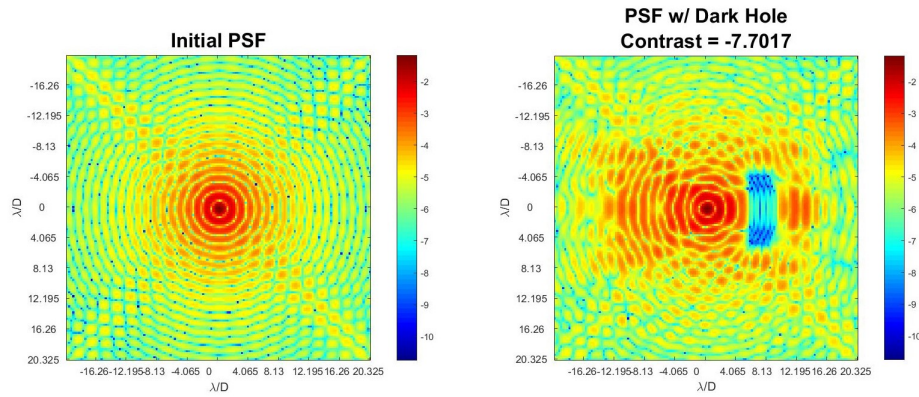


Figure 17: Dark hole with $10^{-7.7}$ contrast that has been created within the stellar PSF using EFC.



References

- [1] G. Singh, J. Lozi, O. Guyon, P. Baudoz, N. Jovanovic, F. Martinache, T. Kudo, E. Serabyn, and J. Kuhn, “On-sky demonstration of low-order wavefront sensing and control with focal plane phase mask coronagraphs,” *Publications of the Astronomical Society of the Pacific* **127**(955), p. 857, 2015.
- [2] ALPAO, “Deformable mirrors,” tech. rep., 2017.
- [3] T. D. Groff, A. J. Eldorado Riggs, B. Kern, and N. Jeremy Kasdin, “Methods and limitations of focal plane sensing, estimation, and control in high-contrast imaging,” *Journal of Astronomical Telescopes, Instruments, and Systems* **2**(1), p. 011009, 2015.